

Role of left-hand cut contributions on pole extractions from lattice data: Case study for $T_{cc}(3875)^+$

Meng-Lin Du¹, Arseniy Filin², Vadim Baru², Xiang-Kun Dong^{3,4}, Evgeny Epelbaum^{1,2}, Feng-Kun Guo^{3,4,5}, Christoph Hanhart⁶, Alexey Nefediev^{7,8}, Juan Nieves⁹ and Qian Wang^{10,11,12}

¹School of Physics, University of Electronic Science and Technology of China, Chengdu 611731, China

²Institut für Theoretische Physik II, Ruhr-Universität Bochum, D-44780 Bochum, Germany

³CAS Key Laboratory of Theoretical Physics, Institute of Theoretical Physics, Chinese Academy of Sciences, Beijing 100190, China

⁴School of Physical Sciences, University of Chinese Academy of Sciences, Beijing 100049, China

⁵Peng Huanwu Collaborative Center for Research and Education, Beihang University, Beijing 100191, China

⁶Institute for Advanced Simulation, Institut für Kernphysik and Jülich Center for Hadron Physics, Forschungszentrum Jülich, D-52425 Jülich, Germany

⁷Jozef Stefan Institute, Jamova 39, 1000 Ljubljana, Slovenia

⁸CeFEMA, Center of Physics and Engineering of Advanced Materials,

Instituto Superior Técnico, Avenida Rovisco Pais 1, 1049-001 Lisboa, Portugal

⁹Instituto de Física Corpuscular (centro mixto CSIC-UV),

Institutos de Investigación de Paterna, Apartado 22085, 46071, Valencia, Spain

¹⁰Guangdong Provincial Key Laboratory of Nuclear Science, Institute of

Quantum Matter, South China Normal University, Guangzhou 510006, China

¹¹Institute of High Energy Physics, Chinese Academy of Sciences, Beijing 100049, China

¹²Guangdong-Hong Kong Joint Laboratory of Quantum Matter, Southern Nuclear

Science Computing Center, South China Normal University, Guangzhou 510006, China

We discuss recent lattice data for the $T_{cc}(3875)^+$ state to stress, for the first time, a potentially strong impact of left-hand cuts from the one-pion exchange on the pole extraction for near-threshold exotic states. In particular, if the left-hand cut is located close to the two-particle threshold, which happens naturally in the DD^* system for the pion mass exceeding its physical value, the effective-range expansion is valid only in a very limited energy range up to the cut and as such is of little use to reliably extract the poles. Then, an accurate extraction of the pole locations requires the one-pion exchange to be implemented explicitly into the scattering amplitudes. Our findings are general and potentially relevant for a wide class of hadronic near-threshold states.

Introduction.—The last two decades have witnessed the discovery of a large number of the so-called exotic hadronic states in the heavy quark sector that do not fit into the scheme of simple quark models [1–9]. For some of them only particular properties like masses or decays strongly deviate from expectations, for others already the quantum numbers unambiguously indicate their multiquark content—the most prominent representatives of this class are the isotriplet Z_c and Z_b states that decay to a heavy quarkonium plus a single pion. For an overview of the experimental situation see, *e.g.*, [7].

The pressing theoretical question is what clusters the quarks form in these exotic hadrons. One popular scenario is that diquarks and anti-diquarks emerge as relatively compact building blocks carrying a color charge [1, 2]. Then, if there are light quarks in the system, the size of the emerging states is governed by the confinement radius, $\sim 1/\Lambda_{\text{QCD}}$ ($\Lambda_{\text{QCD}} \sim 300$ MeV), and does not depend on the binding energy E_b defined as the difference between the mass of the state and the energy of the closest threshold. Alternatively, the building blocks could be color-neutral conventional hadrons. Then, the size of these so-called hadronic molecules is given by the inverse of the binding momentum $\gamma = \sqrt{2\mu E_b} \ll \Lambda_{\text{QCD}}$, with μ for the reduced mass, resulting in large radii of near-threshold states. Thus, the size of hadronic

molecules is limited by the binding momentum rather than by the structure of the interaction. This difference in size leads to significant differences in some observables [4]. Because of confinement, only color singlet multi-hadron intermediate states can go on-shell thereby generating a unitarity or right-hand cut (rhc) in the amplitude. The argument can be further generalized to unstable constituents [10, 11], as long as they are not too broad [12], with lifetime larger than the range of forces [13].

So far little is known about the potential that leads to exotics—this changes with identifying the potentially strong impact of left-hand cuts (lhcs) from the one-pion exchange on the pole extraction for doubly heavy near-threshold states, which is demonstrated here for the first time. For concreteness, we present our findings with the focus on the double-charm meson T_{cc}^+ reported in [14, 15] and treated as a DD^* molecule. Among many exotic candidates, the T_{cc}^+ is of particular interest since its width, apart from a tiny electromagnetic contribution, stems almost entirely from the only available strong decay channel $DD\pi$. Then, the only relevant cut of the amplitude on the real axis is the three-body $DD\pi$ cut (blue dashed vertical lines in Fig. 1), while the DD^* branch cut (green dashed vertical line) splits into a pair of cuts on the second sheet in the complex energy plane [16, 17]. The

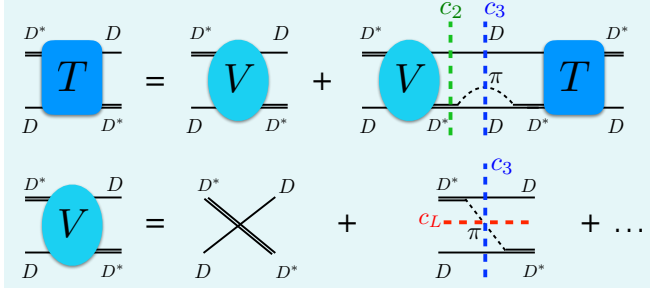


FIG. 1. The cut structure in the DD^* system: (i) the blue dotted vertical lines (c_3) indicate the three-body right-hand cuts, (ii) the green dotted vertical line (c_2) shows the two-body cut, and (iii) the red dotted horizontal line (c_L) is for the left-hand cut. T and V denote the amplitude and interaction potential, respectively.

branch point of the $DD\pi$ cut is located below the nominal DD^* threshold.

The cut structure of the amplitude severely changes for a heavier pion, which can be studied using lattice QCD and chiral effective field theories. As soon as the pion mass m_π exceeds the D^*-D mass difference $\Delta M = M_{D^*} - M_D$, the T_{cc}^+ is stable with respect to the strong interaction, the $DD\pi$ three-body cut branch point appears above the DD^* two-body threshold, and the pion exchange induces the lhc (the red dashed horizontal line in Fig. 1) [18, 19]. Since the location of the branch point is related to the range of the potential and the discontinuity depends on its strength, the lhc is also called dynamical [20]. Other relevant cuts present in the system are discussed below.

The T_{cc}^+ was recently studied in lattice QCD [21–23]. The last work employs the HAL QCD method to extract the DD^* scattering potential and then use it to calculate the phase shifts above the two-body threshold. Our consideration does not directly apply to that approach. In the first two works the Lüscher method is employed to extract the DD^* phase shifts $\delta(E)$ at $m_\pi = 280$ and 350 MeV, respectively. However, in [22], there is only one data point in the near-threshold region and only a single lattice volume is investigated, so the authors themselves argue that a proper discussion of the pole structure of the amplitude is not possible yet. Therefore, we stick to the phase shifts extracted in [21] and related to the scattering T -matrix as

$$-\frac{2\pi}{\mu}T^{-1}(E) = p \cot \delta - ip, \quad (1)$$

with E and p the energy and the magnitude of the relative momentum in the center-of-mass (c.m.) frame, respectively. A pole of the T -matrix appears if

$$p \cot \delta = ip. \quad (2)$$

To exploit condition (2), the phase shifts extracted

from the lattice calculations were parameterized retaining the first two terms in the effective range expansion (ERE) [24],

$$p \cot \delta = \frac{1}{a} + \frac{1}{2}rp^2 + \mathcal{O}(p^4), \quad (3)$$

where a and r are the scattering length and effective range, respectively. However, the convergence radius of ERE is set by the location of the nearest singularity irrespective of its origin. We argue that, in the settings of [21], the physics related to the lhc is relevant and cannot be ignored. In particular, we demonstrate that the simple approximation (3) has to be abandoned in favor of the exact solution of the dynamical equation in the presence of pions, which have a strong effect on both $p \cot \delta$ and the extracted pole. Thus, the physics discussed in this Letter is related to the lhcs from long-range potentials and is quite general.

Importantly, the phase shifts extracted from the lattice data and employed in our analysis may need to be revisited since the presence of the lhc requires a modification of the Lüscher method [25, 26] and may induce sizable partial-wave mixing effects [27]. Being unable to assess quantitatively the importance of these effects, we take the phase shifts extracted above the lhc for granted.

Cut structure of the DD^ amplitude.*—In line with the lattice setting employed to analyze the DD^* system, we work in the isospin limit and use isospin-averaged masses for all mesons. Then the $T_{cc}(3875)^+$ is a purely isoscalar state. The relevant degrees of freedom are DD^* and $DD\pi$, introducing two- and three-body branch points in the amplitude, respectively. For the physical pion mass, pions contribute to the DD^* dynamics in two ways: through the D^* selfenergy and DD^* scattering potential. Both induce rhcs to the amplitude (upper and lower blue dashed vertical lines in Fig. 1, respectively). The three-body $DD\pi$ Green's function generating the most relevant cut in the DD^* scattering amplitude reads [28–31] (for details on time-ordered perturbation theory see, e.g., [32–34])

$$\begin{aligned} G_\pi^{-1}(E, \mathbf{k}', \mathbf{k}) &= E - E_D(k^2) - E_D(k'^2) - \omega_\pi(q^2) \\ &\approx E - 2M_D - \frac{k^2 + k'^2}{2M_D} - \omega_\pi(q^2), \end{aligned} \quad (4)$$

where E is the total energy, \mathbf{k} (\mathbf{k}') is the incoming (outgoing) DD^* relative momentum in the c.m. frame, $E_D(k) = \sqrt{M_D^2 + k^2}$, $\omega_\pi(q^2) = \sqrt{m_\pi^2 + q^2}$, with $\mathbf{q} = \mathbf{k} - \mathbf{k}'$, and $k^{(\prime)} = |\mathbf{k}^{(\prime)}|$, $q = |\mathbf{q}|$.

For the physical pion mass, $m_\pi < \Delta M$, and one can find real values of k and k' such that $G_\pi^{-1} = 0$ for each energy E above the three-body threshold $E_{\text{thr}} \equiv 2M_D + m_\pi$, with the interpretation of the $DD\pi$ state going on-shell. At the same time, the DD^* Green's function has two branch points in the complex s plane ($s = E^2$), giving rise to the two-body unitarity cuts in the scattering amplitude—see Fig. 2 (b).

If m_π increases, ΔM , governed by heavy-quark spin symmetry violation and not chiral dynamics, changes very little, but the phase space for the $DD\pi$ state shrinks. For $m_\pi > \Delta M$, D^* becomes stable (its radiative decays are not considered in lattice calculations, so we neglect them too), and the DD^* branch cut moves to the real axis. We measure the energy relative to the DD^* threshold to write $E = M_{D^*} + M_D + p^2/(2\mu)$, where $\mu = M_{D^*}M_D/(M_{D^*} + M_D)$. The two-body branch point is located at $E = M_D + M_{D^*}$, which implies

$$p_{\text{rhc}_2}^2 = 0. \quad (5)$$

Then,

$$G_\pi^{-1}(E, \mathbf{k}', \mathbf{k}) = \Delta M + \frac{p^2}{2\mu} - \frac{k^2 + k'^2}{2M_D} - \omega_\pi(q^2), \quad (6)$$

so the three-body branch point (we set $k = k' = 0$) is

$$p_{\text{rhc}_3}^2 = 2\mu(m_\pi - \Delta M). \quad (7)$$

In addition, new singularities emerge from (6) in the on-shell partial-wave amplitudes at imaginary values of the momenta, $k^2 = k'^2 = p^2 < 0$. The smallest in magnitude value of p^2 where this happens ($\mu \approx M_D/2$) is given by $\omega_\pi(4p^2) \approx \Delta M$ (backward scattering),

$$(p_{\text{lhc}}^{1\pi})^2 \approx \frac{1}{4}[(\Delta M)^2 - m_\pi^2]. \quad (8)$$

This sets the location of the branch point for the lhc nearest to the threshold. The other, remote, end-point of this lhc is set by forward scattering [34]. The cut structure in the complex s plane for $m_\pi > \Delta M$ (stable D^*) is shown in Fig. 2 (a) with the lhc located below the two-body DD^* threshold. Decreasing m_π , the lhc shrinks and moves towards the threshold. For $m_\pi = \Delta M$ both branch points of the lhc and 3-body rhc (see (7)) hit the threshold. After that, as the D^* becomes unstable, the only relevant cut left on the real axis is the 3-body $DD\pi$ cut—see Fig. 2 (b). Meanwhile, the other possible lhcs from the two-pion or heavier meson exchanges may still be present. Those are much further away from the threshold and irrelevant to the discussion here.

A lhc introduces nonanalyticity to $p \cot \delta$ defined in (1) and, accordingly, sets the upper bound on the convergence radius of ERE (3). For the case at hand, $p \cot \delta$ acquires an imaginary part for energies below the lhc and cannot be treated as real-valued.

Results and discussion.—For an illustration of the general concept, we focus on the lattice data from [21] collected at $m_\pi = 280$ MeV, $M_D = 1927$ MeV and $M_{D^*} = 2049$ MeV (the second data set provided in [21] leads to analogous results [34]). Then, with $\Delta M = 122$ MeV $< m_\pi$, we find

$$(p_{\text{lhc}}^{1\pi})^2 = -(126 \text{ MeV})^2 \implies \left(\frac{p_{\text{lhc}}^{1\pi}}{E_{DD^*}}\right)^2 = -0.0010, \quad (9)$$

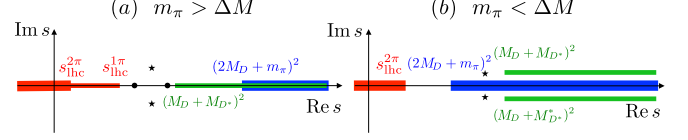


FIG. 2. Sketch of the locations of various branch cuts and poles in the complex s -plane for: (a) $m_\pi = 280$ MeV and (b) the physical pion mass. The left-hand, two-body DD^* , and three-body $DD\pi$ cuts are shown in red, green, and blue, respectively. The black symbols show typical locations for the T_{cc}^+ poles: they can correspond to a pair of virtual states (dots) or a resonance (stars) in case (a) and to a quasi-bound state, which would be a bound state for stable D^* , in case (b). In cases (a) and (b), the poles are on the second and first Riemann sheets, respectively, with respect to the DD^* cut.

where $E_{DD^*} = M_D + M_{D^*}$. In Fig. 3 the location of this lhc branch point is indicated with the dashed vertical line. The $DD\pi$ rhc branch point is located far away,

$$p_{\text{rhc}_3}^2 = (552 \text{ MeV})^2 \implies \left(\frac{p_{\text{rhc}_3}}{E_{DD^*}}\right)^2 = +0.019, \quad (10)$$

and is irrelevant for the current analysis.

In [21] the T -matrix pole is extracted from the lattice data using a linear (in p^2) fit, as defined in (3), in the full energy range, thereby yielding a pole location at $p_0^2/(2\mu) = -9.9$ MeV [$(p_0/E_{DD^*})^2 = -0.0012$], on the second Riemann sheet of the complex s plane. In Fig. 3 this fit is shown as the gray line including its 1σ uncertainty band in light gray. Thus, the pole extracted using only the first two terms in ERE is located below the lhc. However, since the lhc sets the radius of convergence of ERE, the latter is only valid in a small range $|(p/E_{DD^*})^2| < 0.0010$, where no lattice data exist. Furthermore, the central values of the two data points crucial for the fit lie below the lhc, though $p \cot \delta$ should be complex in this case. Therefore, this pole extraction procedure cannot be regarded as reliable.

To improve on the extraction of the pole parameters from the phase shifts we fit the lattice data from [21] with an amplitude that includes the lhc [35]. More precisely, we solve the DD^* scattering equation employing a potential that incorporates the OPE and two contact terms (one momentum-independent and one momentum-dependent) treated as fitting parameters. This is a simplified version of the full amplitude of [31], where D waves are now switched off to be in line with [21]. The chiral extrapolation of the pion decay constant is considered using chiral perturbation theory [36] and that of the $D^*D\pi$ coupling is taken from [37, 38]. To reliably extract the T -matrix pole, the amplitude needs to be put into a finite volume to determine the parameters directly from a fit to the lattice energy levels; however, to demonstrate the effect of the lhc it is sufficient to fit to the existing lattice data. The results are shown in Fig. 3 in red with

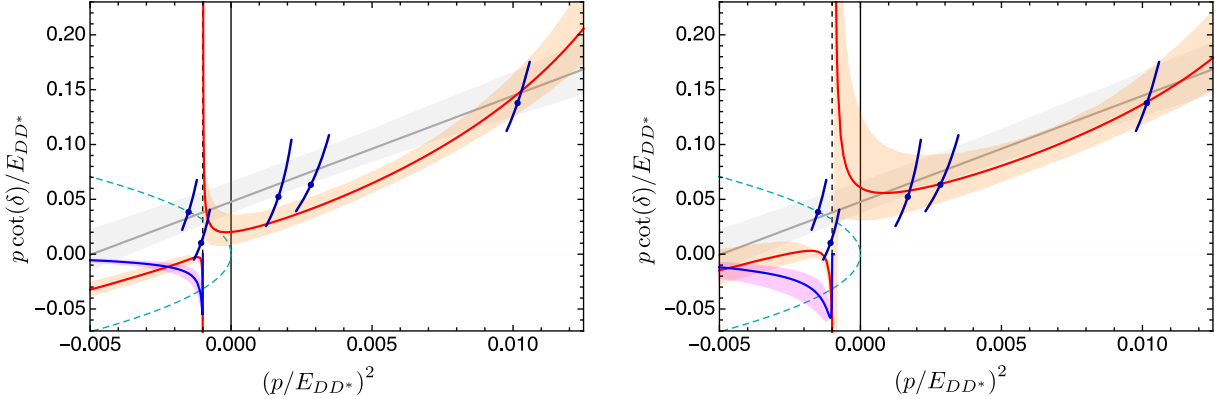


FIG. 3. Fit results for the lattice data from [21]. The solid and dashed vertical lines indicate the DD^* threshold and the lhc, respectively, while the green dashed curve shows the function ip . The gray line and gray band show the fit and its 1σ uncertainty, respectively, found in [21] using ERE formula from (3) in the entire energy range both above and below lhc. The red solid line and the orange band show the best fit and its 1σ uncertainty, respectively, calculated in this work. In the right panel, only the three most right data points were used in the fit while in the left panel, in addition, a part of the error bar of the fourth (from right to left) point located above the lhc (for $(p/E_{DD^*})^2 > -0.0010$) is included in the fit for illustrative purpose. Below the lhc, $p \cot \delta$ acquires an imaginary part, which is shown as the blue line with the pink uncertainty band.

orange uncertainty band [39]. Uncertainty in [21] is given by the probability distribution for each phase shift data point. The nonzero probability of real phase shift data below the lhc is an artifact of the lhc being ignored in [21]. Therefore, the lowest data point in [21] is discarded in our analysis. We perform two fits: one where we use the part of the second data point that is above the lhc (left panel of Fig. 3) and the other one where we ignore it (right panel of Fig. 3). The upper three data points are included in both fits.

The poles of the T -matrix are now extracted using (2). From the left panel of Fig. 3 we conclude that, for the majority of the 1σ parameter space including the best fit, the amplitude contains two virtual states, both residing closer to the DD^* threshold than the pole extracted in [21], where only a single virtual state was found. Those fits within the 1σ band, where $p \cot \delta$ does not cross the ip curve above the lhc, describe the presence of a very narrow resonance showing up as a pair of complex poles below the DD^* threshold. The appearance of a pair of virtual states is natural near the point where they are about to turn to a narrow resonance, as discussed in detail in [40–43]. The position of the lhc sets the upper bound on the virtual pole binding energy—the collision between the virtual pole and its counterpart always takes place between the lhc branch point and the two-body threshold. The fit results presented in the right panel of Fig. 3 are also consistent with the picture just drawn, with the narrow resonance scenario preferred.

In both fits $p \cot \delta$ contains a near-threshold pole as a result of a subtle interplay of the repulsive OPE and the attractive short-range interaction. According to (1), this pole manifests itself as a zero in the T -matrix and provides yet another illustration that, in the current set-

ting, $p \cot \delta$ cannot be approximated by a polynomial with a finite number of terms. Moreover, it emphasizes the important role played by the OPE for understanding the analytic structure of the scattering amplitude. The existence of such a pole in $p \cot \delta$ for the neutron-deuteron scattering was already investigated half a century ago [44, 45]. Here the location of the pole in $p \cot \delta$ very close to the lhc branch point is dictated by the particular lattice data points taken from [21]. Indeed, while the lhc branch point depends only on the masses involved, the exact location of the pole is sensitive to the interaction strength. If the pion coupling constant is artificially decreased or increased by some factor and the lattice data are refitted to fix the contact terms, the pole in $p \cot \delta$ either disappears below the lhc or moves closer to the two-body threshold [34]. In the latter case, it may impose a stronger constraint on the ERE convergence radius than the lhc branch point.

Concluding remarks.—An interesting question is what our findings imply for the nature of the T_{cc}^+ given an intriguing relationship between the location of a near-threshold bound state pole and the size of the molecular component [46, 47] [48]. This formalism relies on the assumption that the binding momentum γ is by far the smallest scale in the problem. However, the lhc induces an additional small scale, which not only strongly limits the range of applicability of ERE (see [30] for a related discussion), but also calls for an improvement of the entire Weinberg approach to describe the compositeness of a hadronic state [49]. On the other hand, a clear visibility in the amplitude of the lhc induced by the OPE provides an additional strong support for the molecular nature of the $T_{cc}(3875)^+$.

In summary, we have demonstrated that the lhcs from

the long-range interactions, with the nearest one originating from the OPE, strongly restrict the range of validity of ERE in extracting the pole positions of near-threshold states. In order to increase this range and thereby extract the poles reliably, at least the OPE needs to be considered explicitly. Our findings clearly suggest that a direct comparison of the below-threshold energy levels predicted by our formalism, put in a finite volume, with the lattice energy levels should be made. The described feature is general, and we illustrated it by reanalyzing the lattice data of [21] for the $T_{cc}(3875)^+$. The same effect may be operative in other hadronic systems where the lhc appears within the range covered by the theory and should be taken into account not only in lattice studies but also in analytical approaches already for physical parameters. These might include not only BB^* and BB^* , but also $\Sigma(\Lambda)N$, $\Sigma_c^{(*)}\bar{D}^{(*)}$, $ND^{(*)}$, $N\bar{D}^{(*)}$ systems and so forth. Consequently, the effect of the lhc could be of relevance for probing the Σ hyper-nuclei, D -mesic nuclei and the properties of charmed and bottom mesons in nuclear matter. Moreover, the $D\bar{D}^*$ is of particular interest for its obvious similarity to the T_{cc}^+ case studied above. The lattice simulations performed in [50] predict the $X(3872)$ as a shallow bound state (11 ± 7) MeV below the $D\bar{D}^*$ threshold. Within the uncertainty, the X pole may appear either below or above the lhc, so the influence of the latter is hard to foresee, and a reanalysis of the system on the lattice seems necessary.

Lattice QCD enters the era of precise calculations for low-lying near-threshold states, which have been a focus of experimental and theoretical hadron physics for two decades and will clearly remain a hot topic in the fore-

seeable future. Our finding can be crucial in accurately extracting the pole locations of the benchmark systems such as DD^* and $D\bar{D}^*$ from lattice data. Thus, the consequences of taking it into account are potentially very important for understanding various exotic hadrons, *e.g.*, whether they exist and what their internal structure is, from first principles of QCD.

ACKNOWLEDGMENTS

The authors would like to thank Sasa Prelovsek for reading the manuscript and valuable comments. This work is supported in part by the National Natural Science Foundation of China (NSFC) and the Deutsche Forschungsgemeinschaft (DFG) through the funds provided to the Sino-German Collaborative Research Center TRR110 “Symmetries and the Emergence of Structure in QCD” (NSFC Grant No. 12070131001, DFG Project-ID 196253076); by the Chinese Academy of Sciences under Grant No. YSBR-101 and No. XDB34030000; by the NSFC under Grants No. 12125507, No. 11835015, and No. 12047503; by the EU STRONG-2020 project under the program H2020-INFRAIA-2018-1 with Grant No. 824093; by the Spanish Ministerio de Ciencia e Innovación (MICINN) under Grant No. PID2020-112777GB-I00; by Generalitat Valenciana under Grant PROMETEO/2020/023; by BMBF (Contract No. 05P21PCFP1) and by the MKW NRW under the funding code NW21-024-A. A.N. is supported by the Slovenian Research Agency (research core Funding No. P1-0035). Q.W. is also supported by Guangdong Provincial funding with Grant No. 2019QN01X172.

-
- [1] A. Esposito, A. L. Guerrieri, F. Piccinini, A. Pilloni, and A. D. Polosa, Four-Quark Hadrons: an Updated Review, *Int. J. Mod. Phys. A* **30**, 1530002 (2015), arXiv:1411.5997 [hep-ph].
 - [2] R. F. Lebed, R. E. Mitchell, and E. S. Swanson, Heavy-Quark QCD Exotica, *Prog. Part. Nucl. Phys.* **93**, 143 (2017), arXiv:1610.04528 [hep-ph].
 - [3] H.-X. Chen, W. Chen, X. Liu, and S.-L. Zhu, The hidden-charm pentaquark and tetraquark states, *Phys. Rept.* **639**, 1 (2016), arXiv:1601.02092 [hep-ph].
 - [4] F.-K. Guo, C. Hanhart, U.-G. Meißner, Q. Wang, Q. Zhao, and B.-S. Zou, Hadronic molecules, *Rev. Mod. Phys.* **90**, 015004 (2018), arXiv:1705.00141 [hep-ph].
 - [5] Y. S. Kalashnikova and A. V. Nefediev, $X(3872)$ in the molecular model, *Phys. Usp.* **62**, 568 (2019), arXiv:1811.01324 [hep-ph].
 - [6] Y. Yamaguchi, A. Hosaka, S. Takeuchi, and M. Takizawa, Heavy hadronic molecules with pion exchange and quark core couplings: a guide for practitioners, *J. Phys. G* **47**, 053001 (2020), arXiv:1908.08790 [hep-ph].
 - [7] N. Brambilla, S. Eidelman, C. Hanhart, A. Nefediev, C.-P. Shen, C. E. Thomas, A. Vairo, and C.-Z. Yuan, The XYZ states: experimental and theoretical sta-
 - tus and perspectives, *Phys. Rept.* **873**, 1 (2020), arXiv:1907.07583 [hep-ex].
 - [8] F.-K. Guo, X.-H. Liu, and S. Sakai, Threshold cusps and triangle singularities in hadronic reactions, *Prog. Part. Nucl. Phys.* **112**, 103757 (2020), arXiv:1912.07030 [hep-ph].
 - [9] H.-X. Chen, W. Chen, X. Liu, Y.-R. Liu, and S.-L. Zhu, An updated review of the new hadron states, *Rept. Prog. Phys.* **86**, 026201 (2023), arXiv:2204.02649 [hep-ph].
 - [10] E. Braaten and M. Lu, Line shapes of the $X(3872)$, *Phys. Rev. D* **76**, 094028 (2007), arXiv:0709.2697 [hep-ph].
 - [11] C. Hanhart, Y. S. Kalashnikova, and A. V. Nefediev, Lineshapes for composite particles with unstable constituents, *Phys. Rev. D* **81**, 094028 (2010), arXiv:1002.4097 [hep-ph].
 - [12] A. A. Filin, A. Romanov, V. Baru, C. Hanhart, Y. S. Kalashnikova, A. E. Kudryavtsev, U.-G. Meißner, and A. V. Nefediev, Comment on “Possibility of Deeply Bound Hadronic Molecules from Single Pion Exchange”, *Phys. Rev. Lett.* **105**, 019101 (2010), arXiv:1004.4789 [hep-ph].
 - [13] F.-K. Guo and U.-G. Meißner, More kaonic bound states and a comprehensive interpretation of the D_{sJ} states,

- Phys. Rev. D **84**, 014013 (2011), arXiv:1102.3536 [hep-ph].
- [14] R. Aaij *et al.* (LHCb), Observation of an exotic narrow doubly charmed tetraquark, Nature Phys. **18**, 751 (2022), arXiv:2109.01038 [hep-ex].
- [15] R. Aaij *et al.* (LHCb), Study of the doubly charmed tetraquark T_{cc}^+ , Nature Commun. **13**, 3351 (2022), arXiv:2109.01056 [hep-ex].
- [16] R. Blankenbecler, M. L. Goldberger, S. W. MacDowell, and S. B. Treiman, Singularities of Scattering Amplitudes on Unphysical Sheets and Their Interpretation, Phys. Rev. **123**, 692 (1961).
- [17] M. Döring, C. Hanhart, F. Huang, S. Krewald, and U.-G. Meißner, Analytic properties of the scattering amplitude and resonances parameters in a meson exchange model, Nucl. Phys. A **829**, 170 (2009), arXiv:0903.4337 [nucl-th].
- [18] S. C. Frautschi and J. D. Walecka, Pion-Nucleon Scattering in the Mandelstam Representation, Phys. Rev. **120**, 1486 (1960).
- [19] J. A. Oller, *A Brief Introduction to Dispersion Relations*, SpringerBriefs in Physics (Springer, 2019).
- [20] R. Omnès, *Introduction to Particle Physics* (John Wiley & Sons Ltd, London, 1971).
- [21] M. Padmanath and S. Prelovsek, Signature of a Doubly Charm Tetraquark Pole in DD^* Scattering on the Lattice, Phys. Rev. Lett. **129**, 032002 (2022), arXiv:2202.10110 [hep-lat].
- [22] S. Chen, C. Shi, Y. Chen, M. Gong, Z. Liu, W. Sun, and R. Zhang, $T_{cc}^+(3875)$ relevant DD^* scattering from $N_f = 2$ lattice QCD, Phys. Lett. B **833**, 137391 (2022), arXiv:2206.06185 [hep-lat].
- [23] Y. Lyu, S. Aoki, T. Doi, T. Hatsuda, Y. Ikeda, and J. Meng, Doubly charmed tetraquark T_{cc}^+ from Lattice QCD near Physical Point, (2023), arXiv:2302.04505 [hep-lat].
- [24] If one of the scattering particles is unstable, it is convenient to make ERE around the complex branch point connected to the two-body channels [51, 52].
- [25] A. B. Raposo and M. T. Hansen, The Lüscher scattering formalism on the t -channel cut, PoS LATTICE**2022**, 051 (2023), arXiv:2301.03981 [hep-lat].
- [26] S. M. Dawid, M. H. E. Islam, and R. A. Briceño, Analytic continuation of the relativistic three-particle scattering amplitudes, (2023), arXiv:2303.04394 [nucl-th].
- [27] L. Meng and E. Epelbaum, Two-particle scattering from finite-volume quantization conditions using the plane wave basis, JHEP **10**, 051, arXiv:2108.02709 [hep-lat].
- [28] V. Baru, A. A. Filin, C. Hanhart, Y. S. Kalashnikova, A. E. Kudryavtsev, and A. V. Nefediev, Three-body $D\bar{D}\pi$ dynamics for the $X(3872)$, Phys. Rev. D **84**, 074029 (2011), arXiv:1108.5644 [hep-ph].
- [29] M. Schmidt, M. Jansen, and H.-W. Hammer, Threshold Effects and the Line Shape of the $X(3872)$ in Effective Field Theory, Phys. Rev. D **98**, 014032 (2018), arXiv:1804.00375 [hep-ph].
- [30] E. Braaten, L.-P. He, and J. Jiang, Galilean-invariant effective field theory for the $X(3872)$ at next-to-leading order, Phys. Rev. D **103**, 036014 (2021), arXiv:2010.05801 [hep-ph].
- [31] M.-L. Du, V. Baru, X.-K. Dong, A. Filin, F.-K. Guo, C. Hanhart, A. Nefediev, J. Nieves, and Q. Wang, Coupled-channel approach to T_{cc}^+ including three-body effects, Phys. Rev. D **105**, 014024 (2022), arXiv:2110.13765 [hep-ph].
- [32] S. S. Schweber, *An Introduction to Relativistic Quantum Field Theory* (Row, Peterson and Company, Evanston, 1961).
- [33] V. Baru, E. Epelbaum, J. Gegelia, and X. L. Ren, Towards baryon-baryon scattering in manifestly Lorentz-invariant formulation of SU(3) baryon chiral perturbation theory, Phys. Lett. B **798**, 134987 (2019), arXiv:1905.02116 [nucl-th].
- [34] See Supplemental Material for technical details of the left-hand cuts, Lippmann-Schwinger equation, fitting procedure and additional analysis of unphysical cases.
- [35] An important role played by the lhc from pion exchanges for NN scattering at unphysical pion masses was pointed out in [53, 54].
- [36] J. Gasser and H. Leutwyler, Chiral Perturbation Theory to One Loop, Annals Phys. **158**, 142 (1984).
- [37] V. Baru, E. Epelbaum, A. A. Filin, C. Hanhart, U.-G. Meißner, and A. V. Nefediev, Quark mass dependence of the $X(3872)$ binding energy, Phys. Lett. B **726**, 537 (2013), arXiv:1306.4108 [hep-ph].
- [38] D. Becirevic and F. Sanfilippo, Theoretical estimate of the $D^* \rightarrow D\pi$ decay rate, Phys. Lett. B **721**, 94 (2013), arXiv:1210.5410 [hep-lat].
- [39] These results were obtained with the D -meson recoil terms included, however their impact is negligible since the three-body cut (10) is sufficiently remote.
- [40] K. W. McVoy, Virtual states and resonances, Nucl. Phys. A **115**, 481 (1968).
- [41] C. Hanhart, J. R. Peláez, and G. Ríos, Quark mass dependence of the rho and sigma from dispersion relations and Chiral Perturbation Theory, Phys. Rev. Lett. **100**, 152001 (2008), arXiv:0801.2871 [hep-ph].
- [42] F.-K. Guo, C. Hanhart, and U.-G. Meißner, Interactions between heavy mesons and Goldstone bosons from chiral dynamics, Eur. Phys. J. A **40**, 171 (2009), arXiv:0901.1597 [hep-ph].
- [43] C. Hanhart, J. R. Peláez, and G. Ríos, Remarks on pole trajectories for resonances, Phys. Lett. B **739**, 375 (2014), arXiv:1407.7452 [hep-ph].
- [44] A. C. Phillips and G. Barton, Relations between low-energy three nucleon observables, Phys. Lett. B **28**, 378 (1969).
- [45] A. S. Reiner, On the anomalous effective range expansion for nucleon-deuteron scattering in the $S = 1/2$ state, Phys. Lett. B **28**, 387 (1969).
- [46] S. Weinberg, Evidence That the Deuteron Is Not an Elementary Particle, Phys. Rev. **137**, B672 (1965).
- [47] D. Morgan, Pole counting and resonance classification, Nucl. Phys. A **543**, 632 (1992).
- [48] The equivalence of the two approaches was first discussed in [55], generalization to virtual states is provided in [56] and, for a positive effective range to be the case for the lattice analyses of T_{cc}^+ [21, 22], in [57, 58].
- [49] That zeros in the T -matrix invalidate the original Weinberg formalism was discussed in [46, 59, 60].
- [50] S. Prelovsek and L. Leskovec, Evidence for $X(3872)$ from DD^* scattering on the lattice, Phys. Rev. Lett. **111**, 192001 (2013), arXiv:1307.5172 [hep-lat].
- [51] E. Braaten and J. Stapleton, Analysis of $J/\psi\pi^+\pi^-$ and $D^0\bar{D}^0\pi^0$ Decays of the $X(3872)$, Phys. Rev. D **81**, 014019 (2010), arXiv:0907.3167 [hep-ph].
- [52] V. Baru, X.-K. Dong, M.-L. Du, A. Filin, F.-K. Guo, C. Hanhart, A. Nefediev, J. Nieves, and Q. Wang, Effective range expansion for narrow near-

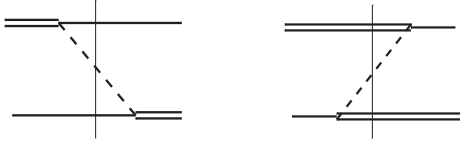


FIG. 4. The two contributions to the OPE interaction between the D^* (double solid line) and D (single solid line) mesons; the dashed line corresponds to the pion. The thin vertical line picks up the relevant intermediate state: $DD\pi$ and $D^*D^*\pi$ for the left and right plot, respectively.

- threshold resonances, *Phys. Lett. B* **833**, 137290 (2022), arXiv:2110.07484 [hep-ph].
- [53] V. Baru, E. Epelbaum, A. A. Filin, and J. Gegelia, Low-energy theorems for nucleon-nucleon scattering at unphysical pion masses, *Phys. Rev. C* **92**, 014001 (2015), arXiv:1504.07852 [nucl-th].
 - [54] V. Baru, E. Epelbaum, and A. A. Filin, Low-energy theorems for nucleon-nucleon scattering at $M_\pi = 450$ MeV, *Phys. Rev. C* **94**, 014001 (2016), arXiv:1604.02551 [nucl-th].
 - [55] V. Baru, J. Haidenbauer, C. Hanhart, Y. Kalashnikova, and A. E. Kudryavtsev, Evidence that the $a_0(980)$ and $f_0(980)$ are not elementary particles, *Phys. Lett. B* **586**, 53 (2004), arXiv:hep-ph/0308129.
 - [56] I. Matuschek, V. Baru, F.-K. Guo, and C. Hanhart, On the nature of near-threshold bound and virtual states, *Eur. Phys. J. A* **57**, 101 (2021), arXiv:2007.05329 [hep-ph].
 - [57] Y. Li, F.-K. Guo, J.-Y. Pang, and J.-J. Wu, Generalization of Weinberg's compositeness relations, *Phys. Rev. D* **105**, L071502 (2022), arXiv:2110.02766 [hep-ph].
 - [58] M. Albaladejo and J. Nieves, Compositeness of S-wave weakly-bound states from next-to-leading order Weinberg's relations, *Eur. Phys. J. C* **82**, 724 (2022), arXiv:2203.04864 [hep-ph].
 - [59] V. Baru, C. Hanhart, Y. S. Kalashnikova, A. E. Kudryavtsev, and A. V. Nefediev, Interplay of quark and meson degrees of freedom in a near-threshold resonance, *Eur. Phys. J. A* **44**, 93 (2010), arXiv:1001.0369 [hep-ph].
 - [60] X.-W. Kang and J. A. Oller, Different pole structures in line shapes of the $X(3872)$, *Eur. Phys. J. C* **77**, 399 (2017), arXiv:1612.08420 [hep-ph].

Appendix A: Theoretical framework and fitting procedure

1. Left-hand cuts from pion exchanges

Here we briefly outline the relation between the pion propagator in the Feynman technique and in the time-ordered perturbation theory (TOPT), for details see, *e.g.*, [32, 33].

We start from the Feynman propagator,

$$D^\pi(q) = \frac{1}{q_\mu q^\mu - m_\pi^2} = \frac{1}{q_0^2 - \omega_\pi^2(q^2)}, \quad (\text{A1})$$

where $\omega_\pi(q^2) = \sqrt{q^2 + m_\pi^2}$, and rewrite it identically in the form

$$D^\pi(q) = \frac{1}{2\omega_\pi(q^2)} \left(\frac{1}{q_0 - \omega_\pi(q^2)} - \frac{1}{q_0 + \omega_\pi(q^2)} \right). \quad (\text{A2})$$

The derivation of the integral equations yields that the energy transfer q_0 in the first and second terms in the parentheses can be substituted as $q_0 = E - E_D(k^2) - E_D(k'^2)$ and $q_0 = -E + E_{D^*}(k^2) + E_{D^*}(k'^2)$, respectively, with \mathbf{k} and \mathbf{k}' for the momenta in the initial and final state, respectively. Then the pion propagator (A2) finally reads

$$\begin{aligned} D^\pi(q) &= \frac{1}{2\omega_\pi(q^2)} \left[\frac{1}{E - E_D(k^2) - E_D(k'^2) - \omega_\pi(q^2)} \right. \\ &\quad \left. + \frac{1}{E - E_{D^*}(k^2) - E_{D^*}(k'^2) - \omega_\pi(q^2)} \right], \end{aligned} \quad (\text{A3})$$

which can be recognized as the TOPT form of the propagator, with the two terms in square brackets for the two time orderings corresponding to the TOPT diagrams shown in Fig. 4.

The lhc branch points from the OPE for the DD^* scattering can be found as the end-point singularities of the $DD\pi$ TOPT Green's function in the on-shell kinematics,

$$\begin{aligned} E - E_D(k^2) - E_D(k'^2) - \omega_\pi(q^2) &\xrightarrow[\text{on shell: } k=k'=p]{\cos \theta = \pm 1} \\ E_{D^*}(p^2) - E_D(p^2) - \omega_\pi(2p^2(1 - \cos \theta)) &\Big|_{\cos \theta = \pm 1} = 0, \end{aligned} \quad (\text{A4})$$

which gives for the lhc branch point near the two-body threshold ($\cos \theta = -1$)

$$\begin{aligned} (p_{\text{lhc}}^{1\pi})^2 &= \frac{1}{4} \left[(\Delta M)^2 - m_\pi^2 \right] \frac{(M_D + M_{D^*})^2 - m_\pi^2}{2M_D^2 + 2M_{D^*}^2 - m_\pi^2} \\ &= \frac{1}{4} \left[(\Delta M)^2 - m_\pi^2 \right] \left[1 + \mathcal{O} \left(\frac{(\Delta M)^2}{M_D^2} \right) \right]. \end{aligned} \quad (\text{A5})$$

Since $\Delta M \ll M_D$, the relativistic correction is negligible for the problem at hand and we arrive at equation (8) in the main text. The position of the more distant branch point corresponding to $\cos \theta = +1$ depends on a particular relation between the masses of the particles involved. In the kinematics discussed in this paper, we have

$$\sqrt{M_D^2 + m_\pi^2} \leq M_{D^*} \leq M_D + m_\pi, \quad (\text{A6})$$

which gives

$$\begin{aligned} (\tilde{p}_{\text{lhc}}^{1\pi})^2 &= \frac{1}{4} \left[(\Delta M)^2 - m_\pi^2 \right] \frac{(M_D + M_{D^*})^2 - m_\pi^2}{m_\pi^2} \\ &= \frac{1}{4} \left[(\Delta M)^2 - m_\pi^2 \right] \frac{4M_D^2}{m_\pi^2} \left[1 + \mathcal{O} \left(\frac{\Delta M}{M_D} \right) \right]. \end{aligned} \quad (\text{A7})$$

It follows from (A5) and (A7) that both lhc branch

points move towards the two-body threshold when m_π decreases, so in the limit $m_\pi = \Delta M$ the lhc disappears. We would like to highlight that the $D^*D^*\pi$ TOPT Green's function generates only a remote lhc for the DD^* scattering that is irrelevant to the discussion and is thus disregarded.

The next in importance lhc comes from the two-pion exchange (TPE) contributions. A rough estimate of its near-threshold branch point can be done if one employs that $(\Delta M)^2/m_\pi^2 \ll 1$ for the lattice settings in [21] to neglect the difference in the mass squared relative to the pion mass squared, which gives $(p_{\text{lhc}}^{2\pi})^2 \approx -m_\pi^2$. This implies that although the TPE contributions may introduce certain corrections, the relatively large distance of $(p_{\text{lhc}}^{2\pi})^2$ from the threshold suggests that there should be no qualitative changes in the extracted poles. Furthermore, it is argued in [53, 54] that a significant portion of the multi-pion-exchange cut contributions is already accounted for through iterations of the OPE.

2. T -matrix

In the isospin limit, the contact potential up to next-to-leading order in the nonrelativistic expansion for the S -wave DD^* isoscalar ($I = 0$) state reads

$$V_C^{I=0}(k, k') = c_0 + c_2(k^2 + k'^2), \quad (\text{A8})$$

where c_0 and c_2 are the low-energy constants and k (k') is the 3-momentum of the incoming (outgoing) particle in the center-of-mass (c.m.) frame. In the framework of the time-ordered-perturbation theory, the one-pion exchange (OPE) potential is written as

$$\begin{aligned} V_{\text{OPE}}^{I=0}(E, k, k') &= \frac{g^2}{8f_\pi^2} \int_{-1}^1 dz D^\pi(E, k, k', z) \\ &\times (k^2 + k'^2 - 2kk'z), \end{aligned} \quad (\text{A9})$$

where, according to (A3),

$$D^\pi(E, k, k', z) = -\frac{D_1(E, k, k', z) + D_2(E, k, k', z)}{2\omega_\pi(q^2)},$$

with

$$\begin{aligned} D_1^{-1}(E, k, k', z) &= 2M_D + \frac{k^2 + k'^2}{2M_D} + \omega_\pi(q^2) - E - i\epsilon, \\ D_2^{-1}(E, k, k', z) &= 2M_{D^*} + \frac{k^2 + k'^2}{2M_{D^*}} + \omega_\pi(q^2) - E - i\epsilon, \end{aligned}$$

and $\omega_\pi(q^2) = \sqrt{m_\pi^2 + k^2 + k'^2 - 2kk'z}$, that is, the pion is treated fully relativistically while the $D^{(*)}$ mesons are nonrelativistic.

The T -matrix (amplitude) is obtained as a solution of the Lippmann-Schwinger equation

$$T(E, k, k') = V(E, k, k') \quad (\text{A10})$$

$$-\int \frac{d^3 q}{(2\pi)^3} V(E, k, q) G(E, q) T(E, q, k'),$$

where the potential is a sum of the contact term and OPE,

$$V(E, k, k') = V_C(k, k') + V_{\text{OPE}}(E, k, k'). \quad (\text{A11})$$

In order to render the integral in (A10) well defined, we set a sharp cutoff Λ . To arrive at the results in Fig. 3, Λ is chosen to be 500 MeV. The DD^* propagator is expressed as

$$G(E, q) = \left[M_{D^*} + M_D + \frac{q^2}{2\mu} - E - \frac{i}{2}\Gamma(E, q) \right]^{-1}, \quad (\text{A12})$$

where $\mu = M_D M_{D^*} / (M_D + M_{D^*})$ is the reduced mass,

$$\Gamma(E, q) = \frac{g^2 M_D}{8\pi f_\pi^2 M_{D^*}} \left[\Sigma(s) - \Sigma_0(s) \theta(M_D + m_\pi - M_{D^*}) \right],$$

with $s = [E - M_D - q^2/(2\mu)]^2$, and

$$\Sigma(s) = \left[\frac{\sqrt{\lambda(s, M_D^2, m_\pi^2)}}{2\sqrt{s}} \right]^3, \quad (\text{A13})$$

where $\lambda(a, b, c) = a^2 + b^2 + c^2 - 2ab - 2bc - 2ca$ is the Källén triangle function. Here

$$\begin{aligned} \Sigma_0(s) &= \Sigma(M_{D^*}^2) \\ &+ 2M_{D^*} \left(E - M_{D^*} - M_D - \frac{q^2}{2\mu} \right) \Sigma'(M_{D^*}^2), \end{aligned}$$

where the first and second terms renormalize the D^* mass and wave function, respectively, if $M_{D^*} < M_D + m_\pi$.

3. Chiral extrapolation of f_π and g

For convenience, we introduce the ratio $\xi = m_\pi/m_\pi^{\text{ph}}$ with m_π^{ph} the physical pion mass. For the masses of the D and D^* we stick to the values used in the lattice calculations and quoted explicitly in [21]. For the pion decay constant f_π , we resort to the result of the one-loop chiral perturbation theory [36] and cast it into the form [37]

$$f_\pi(\xi) = f_\pi^{\text{ph}} \left[1 + \left(1 - \frac{f_0}{f_\pi^{\text{ph}}} \right) (\xi^2 - 1) - \frac{(m_\pi^{\text{ph}})^2}{8\pi^2 f_0^2} \xi^2 \log \xi \right],$$

where $f_0 \equiv f_\pi(m_\pi = 0) = 85$ MeV [38] and $f_\pi^{\text{ph}} = 92.1$ MeV.

For the chiral extrapolation of the $DD^*\pi$ coupling g , we employ the lattice results of [38] and express it in terms of the physical value g^{ph} and $g_0 \equiv g(m_\pi = 0)$ as [37]

$$g(\xi) = g^{\text{ph}} [1 + C_1(\xi^2 - 1) + C_2 \xi^2 \log \xi], \quad (\text{A14})$$

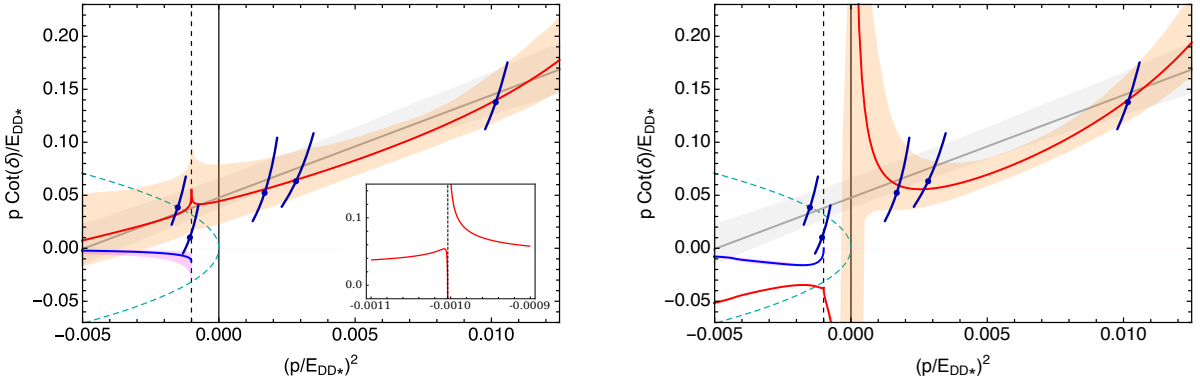


FIG. 5. Fits for the OPE potential artificially suppressed by a factor of 1/10 (the left plot) or artificially enhanced by a factor of 5 (the right plot). The inset in the left panel magnifies the red curve in the vicinity of the lhc branch point. See the caption of Fig. 3 in the main text for further details. Here only the three data points not affected by the lhc are considered in the fits.

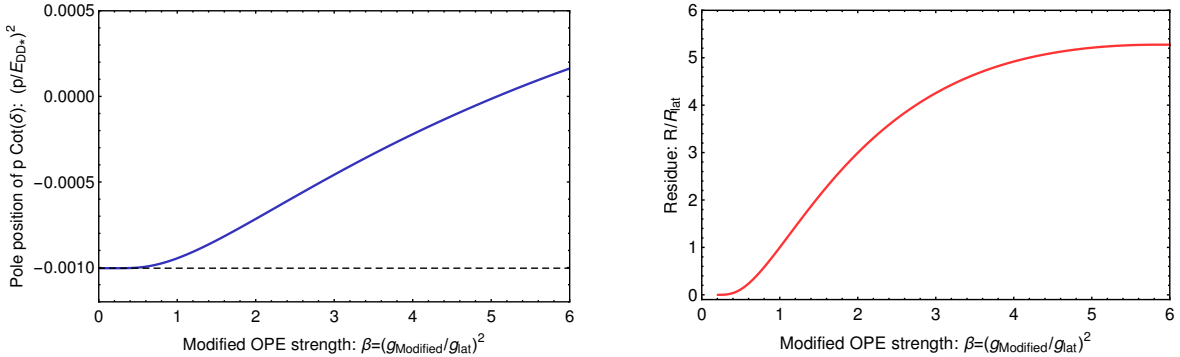


FIG. 6. The behavior of the pole position (left) and the residue (right) of $p \cot \delta$ with the variation of the OPE strength while keeping the pion mass fixed. Only the central values are shown. The horizontal dashed line in the left panel indicates the lhc. The data points used in the fits for the artificially suppressed/enhanced OPE potential are the same as Fig. 5.

where $g^{\text{ph}} = 0.57$ is determined from the experimentally measured $D^{*+} \rightarrow D^0 \pi^+$ decay width [31],

$$C_1 = 1 - \left[1 - \frac{1 + 2g_0^2}{8\pi^2 f_0^2} (m_\pi^{\text{ph}})^2 \log \frac{m_\pi^{\text{ph}}}{\mu_{\text{lat}}} + \alpha_{\text{lat}} (m_\pi^{\text{ph}})^2 \right]^{-1},$$

$$C_2 = -\frac{1 + 2g_0^2}{8\pi^2 f_0^2} (m_\pi^{\text{ph}})^2 (1 - C_1),$$

and the parameters take the values [38]

$$g_0 = 0.46, \quad \alpha_{\text{lat}} = -0.16 \text{ GeV}^{-2}, \quad \mu_{\text{lat}} = 1 \text{ GeV}.$$

Specifically, for $m_\pi = 280$ MeV this gives

$$g(m_\pi = 280 \text{ MeV}) = 0.65. \quad (\text{A15})$$

The variation of the strength of the OPE potential (within approximately 30%, driven by the pion mass dependence of both f_π and g) due to changing m_π between its physical and lattice values provides only a subleading effect on the dynamics of the system at hand while the leading effect comes from the position of the lhc branch

point, as given in (8). Specifically, for $m_\pi > \Delta M$ the lhc is on the real axis in the energy plane with the lhc branch point being close to the threshold.

4. Fitting procedure

In this appendix we describe the procedure employed to fit $p \cot \delta(p^2)$ extracted from the lattice data in [21] using the model described above which explicitly takes into account the OPE interaction.

In particular, the function $p \cot \delta(p^2)$ is related to the DD^* S -wave on-shell scattering T -matrix $T(E)$ as

$$p \cot \delta(p^2) = -\frac{2\pi}{\mu} T^{-1}(E) + ip, \quad (\text{A16})$$

where $T(E) \equiv T(M_D + M_{D^*} + p^2/(2\mu), p, p)$ is a solution of the Lippmann-Schwinger equation (A10).

Since the lattice data points for $p \cot \delta(p^2)$ are extracted using the Lüscher method, their uncertainties have non-Gaussian shapes, which prevents us from per-

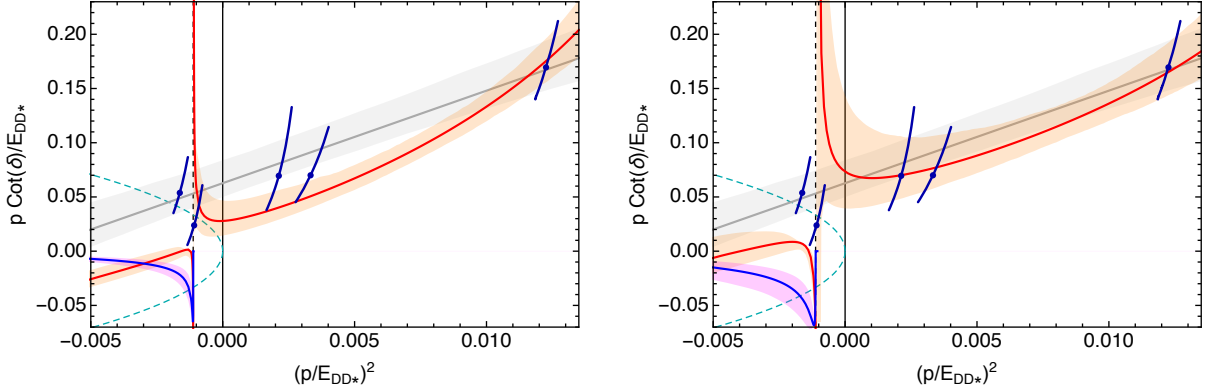


FIG. 7. Fits for the alternative set of parameters provided in [21] and quoted in (B1). See the caption of Fig. 3 in the main text for further details.

forming a naive χ^2 fit. Instead, we employ the probability distribution extracted for each lattice data point from [21] and generate 1000 sets of quasi-data points according to these distributions. Each generated set (with 3 or 4 data points depending on the fit) is then fitted with our model by minimizing

$$\chi^2 = \sum_i \left(p_i \cot \delta(p_i^2) \Big|_{\text{model}} - p_i \cot \delta(p_i^2) \Big|_{\text{quasi-data}} \right)^2$$

as a function of the parameters c_0 and c_2 , where i enumerates the data points used in the fit—see the main text for the details of the selection procedure of the data points. The resulting 1000 pairs $\{c_0, c_2\}$ are used then to evaluate the most probable values of these low-energy constants, $p \cot \delta(p^2)$, and the corresponding 68% confidence intervals. The correlations between lattice data points are not available in [21], so that we do not consider them in our fits. It is sufficient for the illustrative purpose of the significant impact of the OPE potential on the pole extraction as we do not aim at a strict and comprehensive analysis of the lattice data from [21], which calls for a well-justified approach taking the lhc into account.

5. Pionic dynamics for unphysically small and large pion coupling

Here we discuss the effect of the pionic dynamics in case of the OPE potential artificially suppressed by a factor of 1/10 (the left plot in Fig. 5) or enhanced by a factor of 5 (the right plot in Fig. 5). From these plots, in agreement with the natural expectations, one can see that, for a weaker pion exchange, the fit approaches the ERE linear formula. On the contrary, for the enhanced OPE

interaction, the singularity of $p \cot \delta(p^2)$ moves closer to the two-body threshold, thus limiting the range of convergence of the ERE even stronger than the lhc. Therefore, an approximate coincidence of the pole in $p \cot \delta$ and lhc, that takes place for the physical value of the pion coupling, comes as a result of fitting the particular data points taken from [21].

In order to show the essential effect of the OPE on the pole of $p \cot \delta$, we demonstrate how the pole moves if we vary the OPE strength while keeping the pion mass fixed—see the left panel in Fig. 6. For the lattice OPE strength from (A15), the pole of $p \cot \delta$ appears just above the lhc. Then, if the pion coupling (labeled as g_{Modified}) is artificially decreased, the pole gradually approaches the lhc. Finally, as the OPE strength vanishes ($\beta = (g_{\text{Modified}}/g_{\text{latt}})^2 \rightarrow 0$), the residue at the pole also vanishes (see the right panel in Fig. 6), ensuring that OPE is essential for producing the pole in $p \cot \delta$.

Appendix B: Analysis of the lattice data for the smaller charm quark masses

In this appendix we provide the fit results for the lattice data from [21] corresponding to the smaller charm quark masses, namely

$$M_D = 1762 \text{ MeV}, \quad M_{D^*} = 1898 \text{ MeV}, \quad (\text{B1})$$

while the pion mass remains the same as before, $m_\pi = 280$ MeV. The obtained 3- and 4-point fits are shown in Fig. 7. In these settings, the lhc position corresponds to $(p/E_{DD^*})^2 = -0.0011$. As stated in the main text, these fits demonstrate essentially the same behaviour as those shown in Fig. 3 and as such lead to the same conclusions.